J. Fluid Mech. (1981), *vol.* 112, *pp.* 71–96
Printed in Great Britain

Velocity measurements close to rippled beds in oscillatory flow

By C. G. DU TOIT
Department of Civil Engineering, University of Stellenbosch

AND J. F. A. SLEATH
Department of Engineering, University of Cambridge

(Received 30 October 1980 and in revised form 2 March 1981)

The results are reported of velocity measurements in oscillatory flow over rippled beds. Velocities were measured with a laser-doppler anemometer in both an oscillating tray rig and an oscillatory flow water channel. Both self-formed and artificial ripples were examined. In addition, some measurements were made with an apparently plane bed with intense sediment motion.

The experimental results were compared with the predictions of Kalkanis (1964), Kajiura (1968), Bakker (1973, 1974) and Sleath (1974). The closest agreement between theory and experiment was obtained with the method of Sleath.

Measurements of the Eulerian drift velocities showed drift towards the adjacent ripple crest in the immediate vicinity of the bed and away from the crest further out.

1. Introduction

A knowledge of the fluid velocity distribution close to the sea bed is of considerable importance to the coastal engineer. Although the solution for laminar oscillatory flow past a plane bed was given by Stokes as long ago as 1851, much less is known about the velocities close to a rippled bed. Unfortunately the sea bed is frequently rippled and rarely plane.

In this paper we will be concerned with ripples produced by wave action alone. The effects of steady currents and tides are not considered. Lyne (1971) has obtained solutions for low height-to-length ratio ripples for both the case $a/L \ll 1$ and for the case $a/L \gg 1$, where a is the amplitude of the fluid oscillation just outside the boundary layer at the bed and L is the wavelength of the ripple. Qualitative support for Lyne's solution for $a/L \ll 1$ has been provided by the flow visualization experiments of Kaneko & Honji (1979).

There seems, however, to be no generally accepted solution for what Bagnold (1946) called 'vortex ripples'. These are the ripples which are most commonly found when the sediment transport is not too intense. Their height-to-length ratio varies from about 0·1 up to about 0·25 and they are characterized by vortex formation in the lee of the ripple crest. Various different approaches may be used to obtain solutions for the velocity distribution with this type of ripple. Firstly, it may be assumed that ripples are just another form of bed roughness and that consequently the technique

used for turbulent boundary layers in steady flow over rough beds may be extended to oscillatory flow. This is the approach adopted by Kajiura (1968), Bakker (1973, 1974) and Jonsson (1980). On the other hand, Sleath (1974, 1975*a*) suggested that the flow might remain laminar to much higher Reynolds numbers than had previously been supposed and that, even if the flow were turbulent, the mean velocity distribution might still be well represented by a laminar solution if the exchange of momentum from one fluid layer to another was dominated by the vigorous mixing produced by the vortices rather than by the much smaller-scale turbulent eddies. Finally, Longuet-Higgins (1981) has put forward a solution based on the 'discrete vortex' method.

There have been a number of experimental studies of the velocity distribution close to beds in oscillatory flow (e.g. Kalkanis 1957, 1964; Jonsson 1963; Horikawa & Watanabe 1968; Sleath 1970; Greated & Manning 1970; Manning 1971; Macdonald 1973; Jonsson & Carlsen 1976; Nakato *et al.* 1977; Bakker & Van Doorn 1978; Beech 1978). With the exception of Nakato *et al.* none of these investigations was made with bed profiles which closely resembled those of naturally occurring ripples. Also, Nakato *et al.* were principally concerned with the measurement of sediment suspension and only two velocity traverses (one above a crest and one above a trough) were made with a bed of sand free to form its own ripples. However, the velocity distribution in the immediate vicinity of the bed is strongly dependent on the bed profile. Thus, although these previous studies are of considerable interest in other respects they do not provide much help in determining which, if any, of the various methods for calculating the velocity distribution is most suitable for the case of real ripples in oscillatory flow.

The first objective of the present tests was to provide data for the velocity distribution close to self-formed ripples on beds of sand in oscillatory flow in order to allow comparison of the various available theories. In addition, tests have been carried out with a fixed rippled bed in order to examine more closely the relative importance of the various flow parameters.

2. Experimental equipment

Experiments were carried out both in an oscillating tray rig and in an oscillatory flow water channel.

The oscillating tray rig is shown in figure 1. It consisted essentially of a flat tray 0·305 m wide and 1·67 m long which was oscillated in its own plane in a tank of still water. The tank was 0·31 m wide and 2·14 m long and the depth of water above the tray was 0·48 m. Simple harmonic motion was created by means of a variable speed motor with feed-back control driving a Scotch Yoke. The tank was divided into three sections by vertical baffles placed 0·46 m from each end and extending down to within about 0·08 m of the bed. The purpose of these baffles was to prevent vortices shed by the end of the tray from propagating into the central test section. Flow under these baffles was inhibited by vertical cylinders, whose cross-sectional area equalled that of the tray, extending down through the water surface in each of the end sections. The cylinders were linked to the tray in such a way that as the tray moved out from one end the cylinder at that end was lowered to compensate for the volume of water displaced, and vice versa. For the tests with beds of sand the average depth of sand in the tray was approximately 0·03 m.

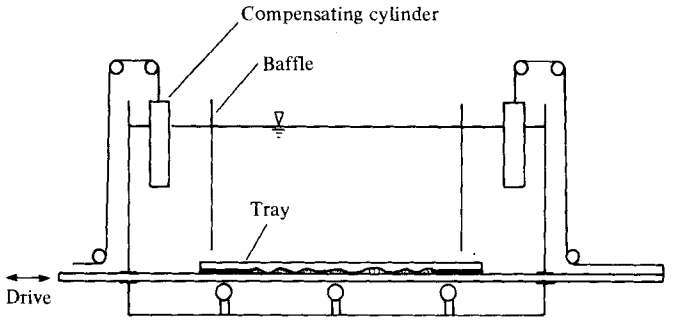

FIGURE 1. Sketch of the oscillating tray rig.

Figure 2 shows a sketch of the oscillatory flow water channel. It consisted of a U-tube in which the water was caused to oscillate by a paddle driven, via a crank arm, by a variable speed motor with feed-back control. The central test section was 0·305 m wide, 0·45 m high and had a length of 3·66 m. The open arm of the U-tube had the same cross-section but the arm containing the paddle was circular in section with an area 3·3 times that of the test section. The walls of the rectangular section of channel consisted of 0·025 m thick Perspex but the circular drum was stainless steel. The average depth of the sediment in the test section was usually about 0·04 m.

The oscillating tray rig had the advantage that it could be operated over a wide range of strokes and periods of oscillation whereas the water tunnel was restricted to periods close to its resonant period of 4·6 s. On the other hand the oscillating tray rig could not be used at high sediment transport rates without significant loss of sand from the bed. Also, it was easy to make velocity measurements down into the trough between crests with the water channel but not with the oscillating bed.

The velocities were measured with a laser-doppler anemometer. A 5 mW Helium–Neon laser was used in forward scatter mode with a Malvern Instruments Frequency shifter and a Cambridge Consultants frequency tracker. Output from the frequency tracker was recorded on magnetic tape and subsequently fed through an analog-to-digital converter into a computer for analysis. The laser and its associated optics were mounted on a milling machine base to allow vertical and horizontal traversing. With the equipment available it was only possible to measure one component of velocity. The results given below are all for the horizontal component of velocity. Calibration was carried out at periodic intervals with the aid of a Feedback FG 601 Function Generator.

The size of the measuring volume containing the interference fringes was 0·3 mm wide, 0·3 mm high and 1·0 mm across the tank in all tests. Since we are concerned with two-dimensional flows the finite size of the measuring volume in the direction across the tank is unlikely to introduce any significant error. However, at right angles to the bed the velocity gradient may be very large so that the finite size of the measuring volume in that direction may not be unimportant. In order to check this point, preliminary velocity measurements were made with a glass plate installed in the oscillating tray rig. Figure 3 shows a typical velocity profile. The close agreement between theory and experiment suggests that the finite size of the measuring volume does not introduce any significant error.

It will be seen from figure 3 that the system of compensating cylinders described

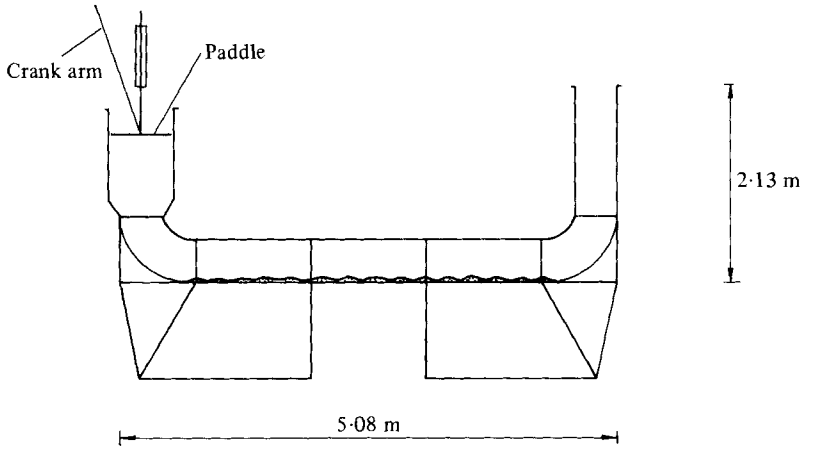

FIGURE 2. Sketch of the oscillating flow water tunnel.

above did not entirely eliminate oscillation of the fluid in the tank outside the boundary layer. The amplitude of this parasitic oscillation was found to vary with period, but for none of the tests with rippled beds did it exceed 5 % of the amplitude of the tray velocity. For an infinite smooth plate oscillating with velocity $U_0 \cos \omega t$ in a semi-infinite fluid it may readily be shown that in laminar flow the fluid velocity u at distance y from the plate is

$$u = U_0 \exp(-\beta y) \cos(\omega t - \beta y) + U_\infty [\cos(\omega t + \phi) - \exp(-\beta y) \cos(\omega t + \phi - \beta y)], \quad (1)$$

where $U_\infty \cos(\omega t + \phi)$ is the fluid velocity at large distances from the plate, ω is angular velocity, t is time and $\beta = (\omega/2\nu)^{\frac{1}{2}}$ where ν is kinematic viscosity. For the test shown in figure 3 the amplitude U_∞ and phase ϕ of the velocity in the fluid at large distances from the bed were determined by direct measurement.

For the oscillating tray rig, phases were measured with the aid of a beam of light falling on a photo-electric cell. A flat plate was attached rigidly to the Scotch Yoke in such a way that the beam of light was interrupted as the tray passed through the top dead-centre position. Output from the photo-electric cell was recorded on magnetic tape and analysed in the same way as the velocity signal. For the oscillatory flow water channel the output from a resistance gauge in the open leg of the tube was used as a phase marker. The phase shift between this signal and the fluid velocity outside the boundary layer was determined by comparing the two signals when the velocity in the test section was being recorded at large distances from the bed. The resistance gauge was also used to check that there was no change in the amplitude and period of fluid oscillation during the course of a test. However, the actual amplitude of the fluid oscillation in the test section was always determined directly from the velocity measurements at large distances from the bed. This avoided the need for complicated corrections for the change in section due to the bed of sand and the boundary layers on the walls.

Fourier analysis of the velocity measurements at large distances from the bed in the test section of the oscillatory flow water channel showed that the free-stream oscillation was not entirely free from harmonics. However, in no test did a harmonic exceed 5·2 % of the fundamental and in most cases harmonics were significantly smaller.

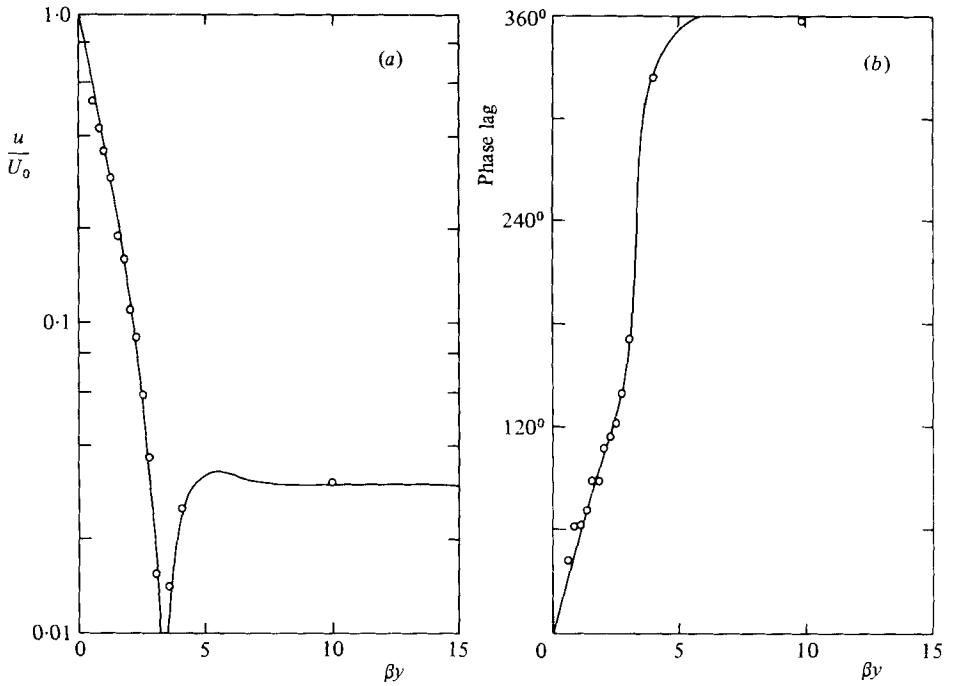

FIGURE 3. Variation with height of (*a*) the amplitude and (*b*) the phase of the velocity over a glass plate in the oscillating tray rig. $U_0/(\omega\nu)^{\frac{1}{2}} = 166{\cdot}6$. ○, measured velocity; ——, theory, equation (1).

Tests were carried out with both self-formed and artificial ripples. Almost all of the tests with self-formed ripples were carried out with a sand of median diameter 0·41 mm and standard deviation 0·10 mm. With this sand the only stable ripples which could be obtained in both the water channel and the oscillating tray were vortex ripples. A number of other sands ranging in diameter from 0·1–1·27 mm were also tested but in no case were stable rolling-grain ripples (i.e. ripples with height-to-length ratios less than about 0·1) obtained. However, it has been suggested that rolling-grain ripples are stable at very high sediment transport rates. Consequently tests were carried out in the water channel with Perspex beads of median diameter 0·6 mm under conditions approaching those of a 'washed-out' bed (i.e. plane bed with very high sediment transport). Unfortunately, useful velocity measurements could only be made when the bed appeared almost plane, since, when well-defined ripples were present, the sediment in suspension obscured the laser beam over almost the entire test section. The specific gravity of the sand was 2·65 and of the Perspex beads was 1·13.

The artificial ripple bed was made out of wood and was machined on a numerically-controlled milling machine to the following profile

$$y = \tfrac{1}{2}h\cos k\xi, \quad x = \xi - \tfrac{1}{2}h\sin k\xi, \tag{2}$$

where the crest-to-trough height h of the ripple was 0·017 m and the wavelength $2\pi/k$ was 0·10 m. This profile is very similar to that of the ripples which form with the 0·41 mm sand. Figure 4 shows a comparison between equation (2) and two of the ripple profiles obtained with the 0·41 mm sand in the oscillating tray rig. These

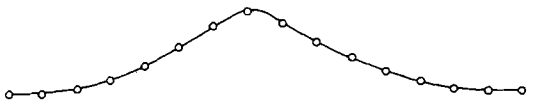

(a)

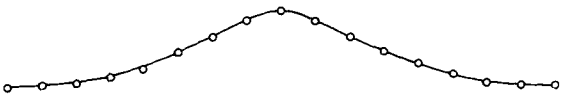

(b)

FIGURE 4. Comparison of equation (2) with ripple profiles measured using 0·41 mm sand. (a) $L = 0{\cdot}138$ m; $h/L = 0{\cdot}17$. (b) $L = 0{\cdot}156$ m; $h/L = 0{\cdot}14$. ○, measured profile; ——, equation (2).

profiles were measured with the tray at rest and may consequently be regarded as mean profiles.

Further details of the experimental equipment are given by Du Toit (1980).

3. Test procedure and results

At least one day prior to the test the tank was filled with tap water and left to de-aerate. With beds of self-formed ripples the appropriate frequency and amplitude of oscillation were selected and the rig was run until the ripples reached their equilibrium profile. The motor was then switched off and the ripple geometry was measured. On the day of the test the equipment was switched on in the morning and left for at least an hour to warm up. A small quantity of milk was then added to the water to provide additional seeding particles for the laser-doppler measurements.

Most of the tests involved two vertical traverses. For each traverse the output from the laser-doppler anemometer was recorded at various fixed heights above the bed for at least thirty cycles. Apart from figures 18 and 19, all of the results presented below are for the average velocity cycle obtained by conditional sampling of thirty recorded cycles. It was found that there was no significant difference between this average cycle and that obtained from the average of sixty recorded cycles.

During the course of the experiment the water temperature was checked at regular intervals as was the output from the various instruments. At the end of the test the ripple geometry was again measured to ensure that there had been no significant change during the course of the test.

The conditions under which the various tests were carried out are summarized in table 1. All of the tests with the self-formed ripples were in the fully-developed rough turbulent regime according to the criteria of Kajiura (1968), Sleath (1974), Kamphuis

a (m)	T (s)	$\frac{a}{L}$	$\frac{h}{L}$	β/k	$\frac{U_0 L}{\nu}$
		(i) *Artificial ripples*			
0·06	3·29	0·6	0·17	15·02	10690·3
0·08	3·25	0·8	0·17	15·22	14637·0
0·10	3·36	1·0	0·17	15·05	17872·9
0·12	3·32	1·2	0·17	15·25	22039·2
0·04	3·47	0·4	0·17	14·94	7049·8
0·02	3·47	0·2	0·17	14·95	3528·1
0·02	1·86	0·2	0·17	19·92	6268·3
0·04	1·87	0·4	0·17	19·98	12603·5
0·06	1·90	0·6	0·17	19·98	18738·0
0·08	1·90	0·8	0·17	19·91	25036·1
0·10	1·89	1·0	0·17	20·03	31668·2
0·12	1·96	1·2	0·17	19·74	36937·0
0·02	5·45	0·2	0·17	12·05	2291·7
0·04	5·46	0·4	0·17	12·06	4593·0
0·06	5·47	0·6	0·17	11·99	6810·8
0·08	5·61	0·8	0·17	11·86	8888·8
0·10	5·66	1·0	0·17	11·86	11097·9
0·12	5·56	1·2	0·17	12·00	13644·6
		(ii) *Self-formed ripples*			
0·060	3·97	0·79	0·13	10·04	6280·7
0·065	3·91	0·72	0·18	12·08	8273·9
0·085	4·73	0·71	0·18	14·99	12570·8
0·110	4·98	0·67	0·17	19·89	20957·5
0·122	5·37	0·71	0·17	19·67	21617·5
0·096	4·22	0·83	0·19	15·05	14898·2
0·101	3·21	0·74	0·20	20·26	23884·0
0·195	4·87	0·77	0·17	30·27	55812·8
0·141	3·18	0·67	0·16	31·05	50935·9
0·081	5·75	0·75	0·19	12·10	8611·9
0·085	4·62	0·86	0·19	12·18	10001·4
0·166	4·65	0·68	0·18	30·54	49852·9
0·108	3·80	0·72	0·20	19·97	22676·9

TABLE 1. Test conditions

(1975) and Jonsson (1980). For the artificial ripples, the criteria of Kamphuis and Kajiura indicate that all of the tests were in the fully-developed rough turbulent regime. On the other hand the criteria of Sleath (1974) and Jonsson suggest that those tests in table 1 for which $a/L = 0{\cdot}2$ and some of those at $a/L = 0{\cdot}4$ were not fully-developed rough turbulent. None of the above criteria are based on measurements for ripple beds. However, the formula of Sleath (1975*b*), which is based on ripple bed measurements, indicates that the tests for $a/L = 0{\cdot}2$ were not turbulent whereas all of the others were. It thus seems reasonable to conclude that the artificial ripple tests in table 1 for which $a/L = 0{\cdot}2$ were not turbulent, those for $a/L = 0{\cdot}4$ were either transition or fully-developed rough turbulent, and those for $a/L \geqslant 0{\cdot}6$ were in the fully-developed rough turbulent regime.

3.1. *Artificial ripples in oscillating tray rig*

The two traverses made during each test will be referred to as traverse A and traverse B. At mid-stroke the measuring volume of the laser-doppler anemometer was directly above a ripple crest for traverse A and directly over a trough for traverse B.

Figure 5 shows an example of the sort of result obtained for the average velocity cycle. Two curves are shown for the test results. If the ripples are symmetrical about a crest (as is the case here) the mean velocity (averaged over a large number of cycles) during one half cycle should, by symmetry, be equal in magnitude but opposite in sign to that in the other half cycle. The dashed line during one half cycle is the 'mirror image' of the full line during the other half cycle. Thus the difference between the two curves provides an indication of the magnitude of experimental errors such as mean drift in the tank. Since the analog-to-digital conversion was carried out at a rate of between 600 and 720 samples per cycle the experimental results are shown as continuous curves.

Also shown are the predictions obtained from the formulae put forward by various workers. Since the flow was probably laminar, agreement between Bakker's method (which assumes turbulent flow) and the experimental results is hardly to be expected. This comment would also apply to Jonsson's formula. However, there is another reason why no comparison is made with Jonsson's formula, either here or in any of the subsequent figures. This is that Jonsson's formula is only valid when there is an overlap layer. According to Kajiura (1968) the overlap layer disappears when $a/k_s < 30$, where k_s is the Nikuradse roughness size. Thus if $k_s = 4\,h$, where h is ripple height, and $h/L = 0{\cdot}17$, which is the value adopted for the artificial ripples, Jonsson's formula cannot be used if $a/L < 20{\cdot}4$. It may be mentioned in passing that Horikawa & Watanabe (1968) suggested that Kajiura's results actually show that the overlap layer disappears when $a/k_s < 115$ (the present authors have repeated the calculation and find the same result). This would mean that, for $h/L = 0{\cdot}17$, Jonsson's formula would only apply when $a/L > 78{\cdot}2$. These limits should be treated with some caution since Kajiura's model is based on the assumption that an overlap layer either exists during the whole of the cycle or not at all. In reality an overlap layer might exist for only part of the cycle. However, the limiting values of a/L are so much greater than those in the present tests (cf. table 1) that any comparison with Jonsson's formula would be meaningless.

The formula put forward by Kalkanis (1964) is purely empirical and was based on the results of his tests with round and half-round rods. In making the comparison shown in figure 5 it has been assumed that the rod diameter D may be replaced in his formula by the wavelength of the ripples. Various other assumptions as to the value to be adopted for D are possible but this is the one which gives the most favourable comparison between Kalkanis' formula and the present test results. In this and subsequent figures, the origin for the velocities is assumed to be $0{\cdot}2\,h$ below the crest level for the formulae of Kalkanis and Kajiura and $0{\cdot}38\,h$ below crest level for Bakker's method. The Nikuradse roughness size k_s is assumed to be $4\,h$ as suggested by Motzfeldt (1937). The curves shown for Bakker's method are for the fundamental component only. However, since the higher harmonics obtained with this method are invariably small it is believed that their inclusion would not significantly affect the comparison.

The method of Sleath is the same as that outlined by Sleath (1974). However, so

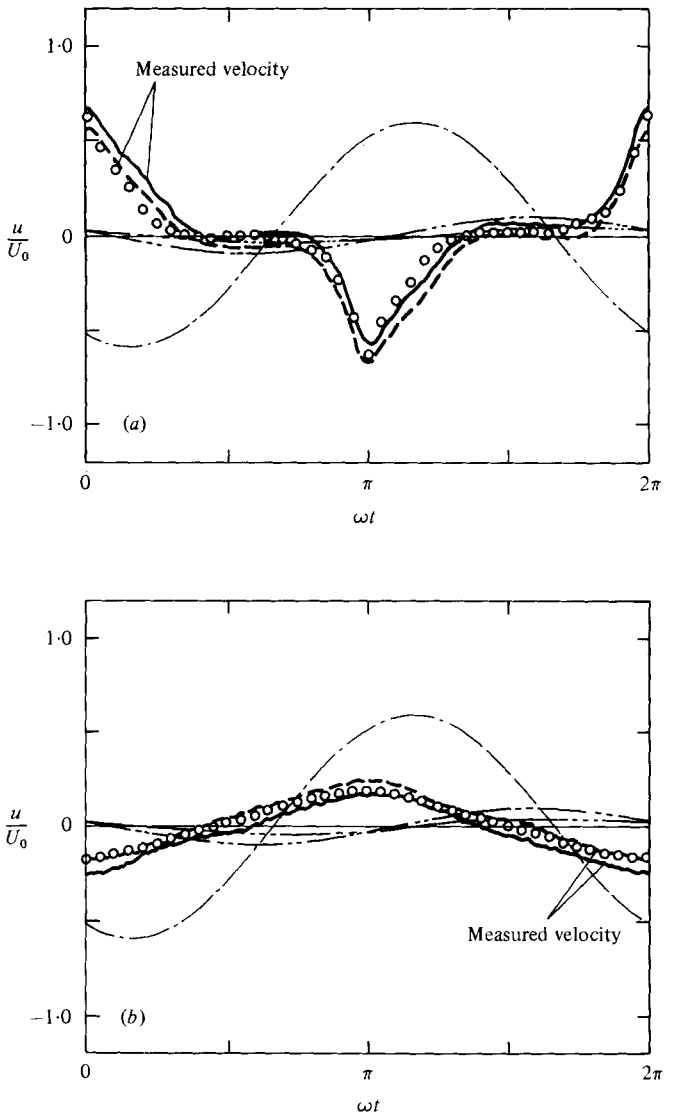

FIGURE 5. Examples of the average velocity cycle using the artificial ripple bed. $a/L = 0{\cdot}2$, $\beta/k = 20$, $\beta y_1 = 3{\cdot}1$. (*a*) Traverse *A*; (*b*) traverse *B*. ——— ———, Kajiura; ——— — ———, Kalkanis; ——— — — ———, Bakker; ○, Sleath.

as to obtain a bed profile more like that of natural ripples the curvilinear co-ordinate system used in the present calculations was

$$\xi = x + \tfrac{1}{2}h\exp(-k\eta)\sin k\xi, \quad \eta = y - \tfrac{1}{2}h\exp(-k\eta)\cos k\xi. \tag{3}$$

If the bed is taken to be $\eta = 0$ this gives the same profile as (2) which, as shown by figure 4, is very similar to that of naturally-occurring ripples. As mentioned by Sleath (1974) the computed velocity ceases to be identical from one cycle to the next when the Reynolds number exceeds a certain limit. This is to be expected since the method consists of a numerical solution of the Navier Stokes equations. Thus, under conditions where the real flow ceases to be identical from one cycle to the next (cf. Sleath

1975*b*) we would not expect the computed flow to remain stable. Consequently, the results shown here have been averaged, in the same way as the experimental results, over a sufficient number of cycles for the mean cycle to be identical from one sample to the next. Most of the computations were made with 800 time steps per cycle. The points shown in figure 5 represent the velocities at the end of each 20 time steps. The mesh spacing in the ξ-direction was the same as that of Sleath (1974) but that in the η-direction was modified to give an outer boundary at $\beta y = 184$.

No comparison has been attempted with the method of Longuet-Higgins (1981) since velocity profiles are not available at the time of writing.

It should be pointed out that y is vertical distance measured from the mean bed level whereas y_1 is measured from the ripple crest. Thus

$$y = y_1 + \tfrac{1}{2}h. \tag{4}$$

A value of $a/L = 0{\cdot}2$ would only be found in practice with a ripple formed under more severe flow conditions and then remaining when the amplitude of oscillation dropped. Figure 6 shows an example of the results obtained with the artificial ripples at $a/L = 1{\cdot}0$. This represents very severe flow conditions for a ripple as steep as this since, although larger values of a/L may be found in practice, they usually correspond to smaller values of h/L.

Comparison of figures 5 and 6 shows that Sleath's method gives very good agreement with the experimental results at low values of a/L but that the agreement becomes less good at high a/L. This is hardly surprising since the assumption in Sleath's method that turbulence does not significantly affect the mean velocity profile will obviously be more reasonable, for given β/k, at low values of a/L than at high values. The way in which the situation changes with increasing a/L is illustrated in figures 7 and 8. Figure 7 shows the maximum value U_m of the horizontal component of velocity during the course of a cycle and figure 8 shows the phase at which this maximum occurs. For traverse B the magnitude of the maximum measured velocity rises to a peak at $a/L = 0{\cdot}6$ and then declines slightly at both $\beta y_1 = 3{\cdot}0$ and $\beta y_1 = 15{\cdot}0$. For traverse A the maximum velocity initially falls slightly but then increases again with increasing a/L at $\beta y_1 = 3{\cdot}0$ whereas it climbs steadily as a/L increases at $\beta y_1 = 15{\cdot}0$. These trends are quite well reproduced in Sleath's computed results but the other three methods all show a steady increase in maximum velocity with increasing a/L.

If only figure 7 were available one would be tempted to conclude that Kajiura's method gave significantly better agreement with the experimental results than either Kalkanis' or Bakker's methods. However, it is clear from figures 5 and 6 that although Kajiura's method gives a reasonable prediction of the magnitude of the maximum velocity its prediction of the phase at which this maximum occurs is poor. This is illustrated by figure 8 which shows that only Sleath's method gives close agreement with the experimental phases. The discontinuous nature of the experimental curve for traverse A arises because, as shown by figure 6, the velocity record has several peaks. At one value of a/L one of these peaks may be the largest whereas at a slightly different value of a/L another peak may dominate.

Finally, figure 9 shows, for traverse A, the way in which the amplitude and phase of the maximum velocity during the course of the cycle vary with βy_1 for various values of a/L. Figure 10 gives the corresponding results for traverse B. It is clear that, with the exception of the two largest values of a/L for traverse B, there is little

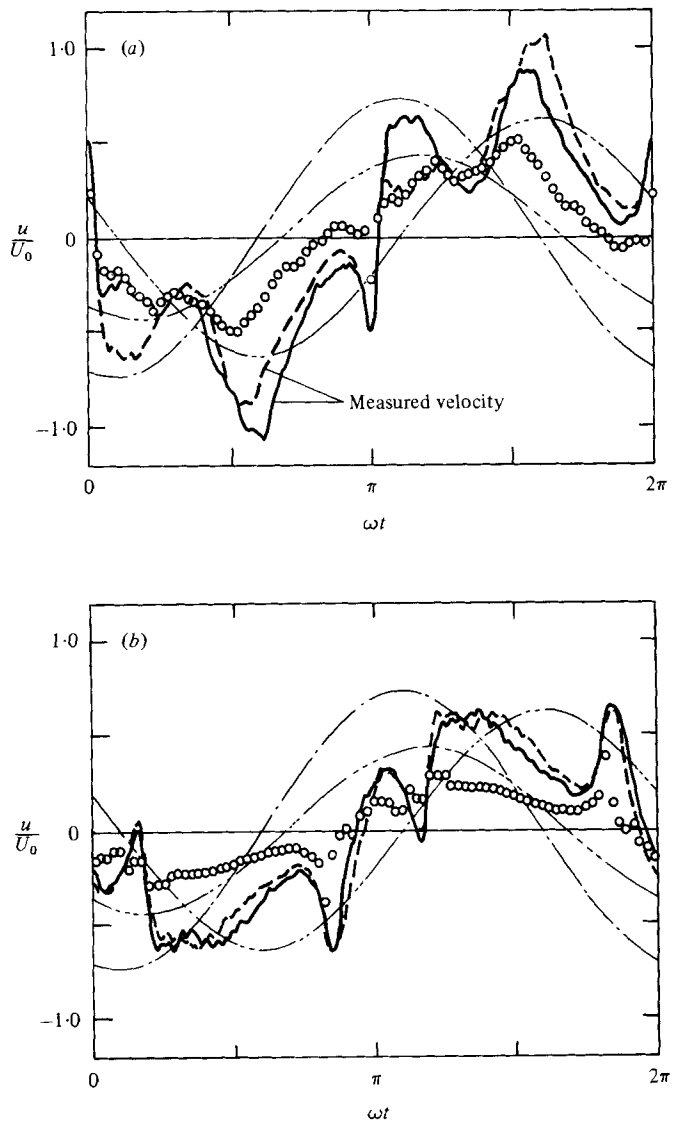

FIGURE 6. Examples of the average velocity cycle using the artificial ripple bed. $a/L = 1{\cdot}0$, $\beta/k = 20$, $\beta y_1 = 3{\cdot}1$. (*a*) Traverse *A*; (*b*) Traverse *B*. For the symbols see figure 5.

variation in phase with βy_1 for given a/L. For this value of β/k there is also little variation in the magnitude of the maximum velocity for the range of y_1 investigated. In order not to confuse these figures the predictions of the various methods are not shown. However, since the variation with βy_1 is generally small the sort of comparison to be expected may be inferred from figures 7 and 8.

All of the discussion so far has been of tests for which $\beta/k = 20$. Similar tests were also carried out at $\beta/k = 15$ and $\beta/k = 12$. Figures 11 and 12 show the way in which the maximum velocity at $\beta y_1 = 3{\cdot}0$ and $\beta y_1 = 15{\cdot}0$ varies with a/L for the three values of β/k. Very close to the bed, i.e. at $\beta y_1 = 3{\cdot}0$, there is hardly any variation in U_m/U_0 with β/k. The influence of β/k is somewhat greater at $\beta y_1 = 15{\cdot}0$ but, even here, the general trends are very much the same for the three values of β/k investigated.

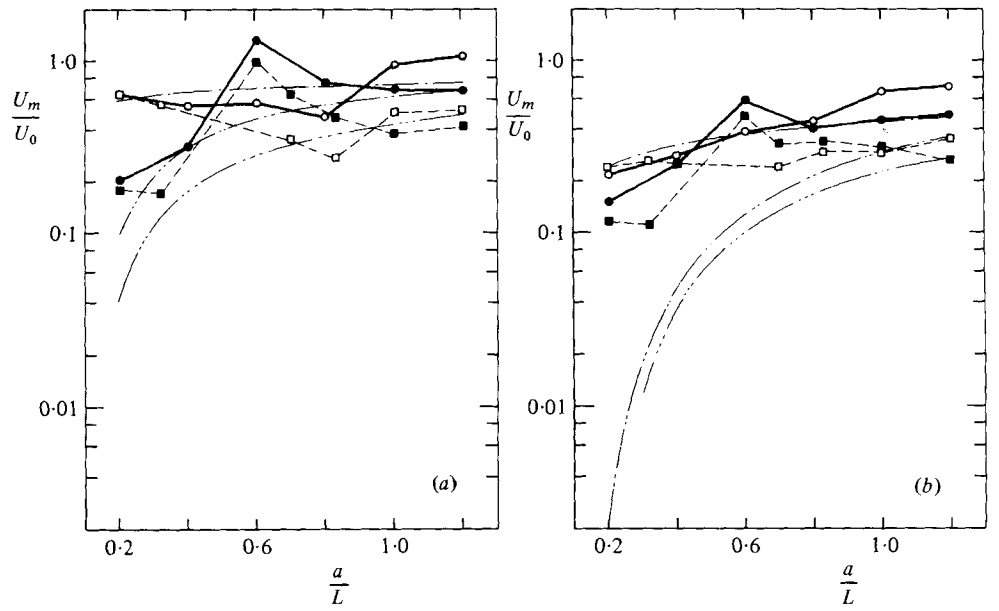

FIGURE 7. Variation with a/L of the magnitude of the maximum velocity during a cycle. (*a*) $\beta y_1 = 3{\cdot}0$, $\beta/k = 20$. (*b*) $\beta y_1 = 15{\cdot}0$, $\beta/k = 20$. ——— ———, Kajiura; ——— · ———, Kalkanis; ——— · · ———, Bakker; ○, traverse *A*, measurement; □, traverse *A*, Sleath; ●, traverse *B*, measurement; ■, traverse *B*, Sleath.

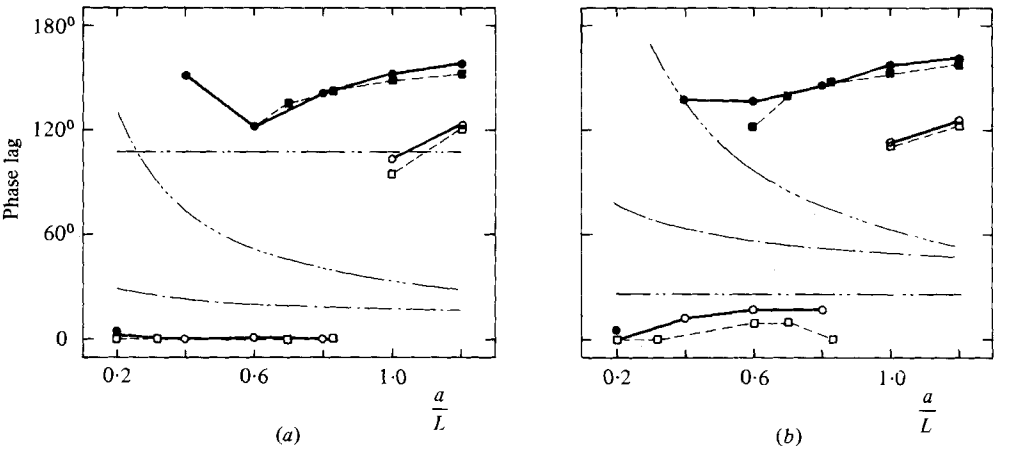

FIGURE 8. Variation with a/L of the phase at which the maximum velocity during a cycle occurs. (*a*) $\beta y_1 = 3{\cdot}0$, $\beta/k = 20$; (*b*) $\beta y_1 = 15{\cdot}0$, $\beta/k = 20$. The symbols are the same as in figure 7.

It might be thought that viscous effects would be relatively unimportant for this sort of flow and that consequently ky_1 would be a more relevant parameter than βy_1 in, say, figures 9 and 10. This is clearly not true in the immediate vicinity of the bed, where viscous effects are highly important. Also, it was found that when the results, such as those shown in figures 9 and 10, were plotted against ky_1 the scatter between curves for different values of β/k was no less than with βy_1 as independent variable.

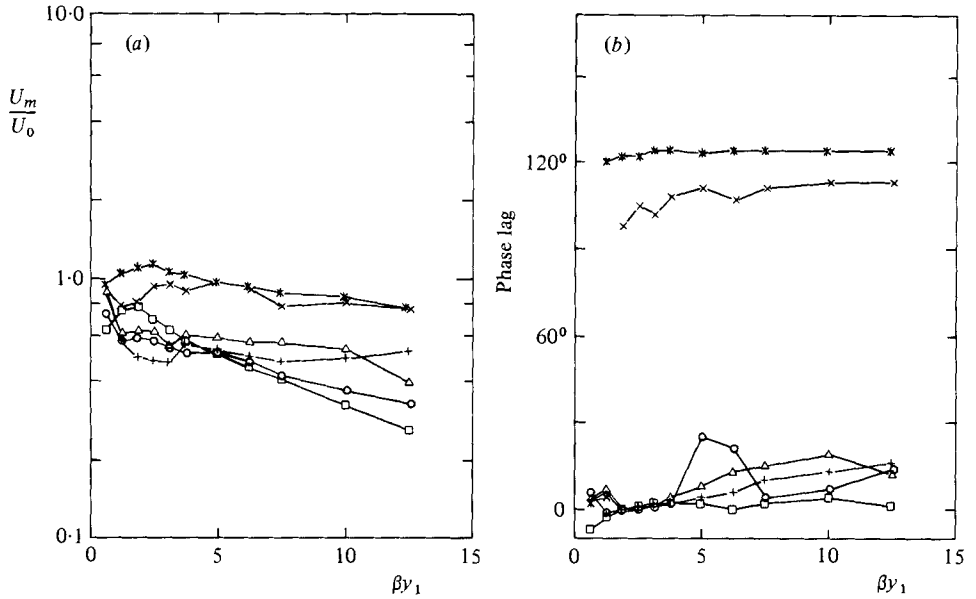

FIGURE 9. Variation with βy_1 of (*a*) the magnitude and (*b*) the phase of the maximum velocity during a cycle. Traverse *A*. $\beta/k = 20$. □, $a/L = 0{\cdot}2$; ○, $a/L = 0{\cdot}4$; △, $a/L = 0{\cdot}6$; +, $a/L = 0{\cdot}8$; ×, $a/L = 1{\cdot}0$; ✳, $a/L = 1{\cdot}2$.

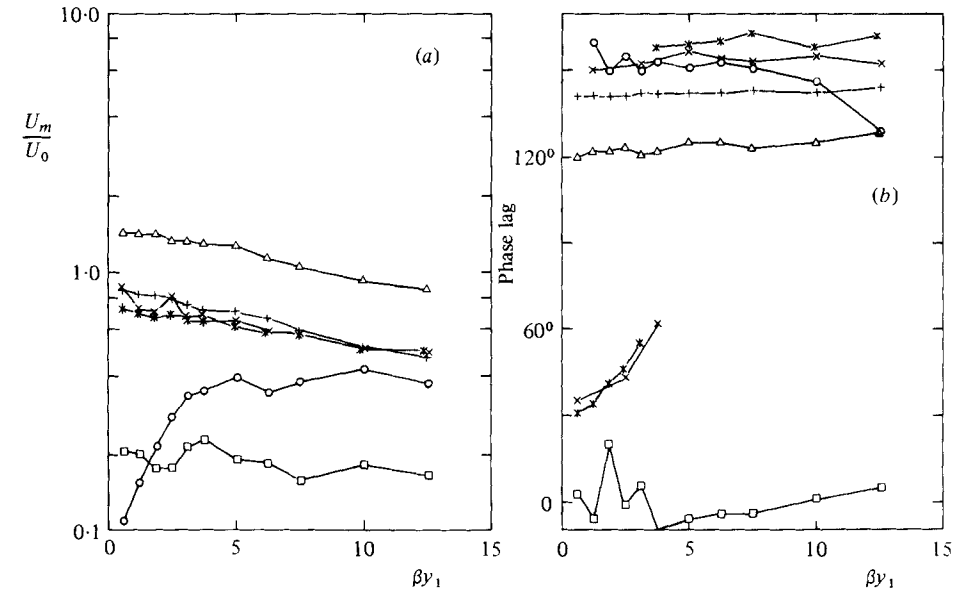

FIGURE 10. Variation with βy_1 of (*a*) the magnitude and (*b*) the phase of the maximum velocity during a cycle. Traverse *B*. $\beta/k = 20$. The symbols are the same as in figure 9.

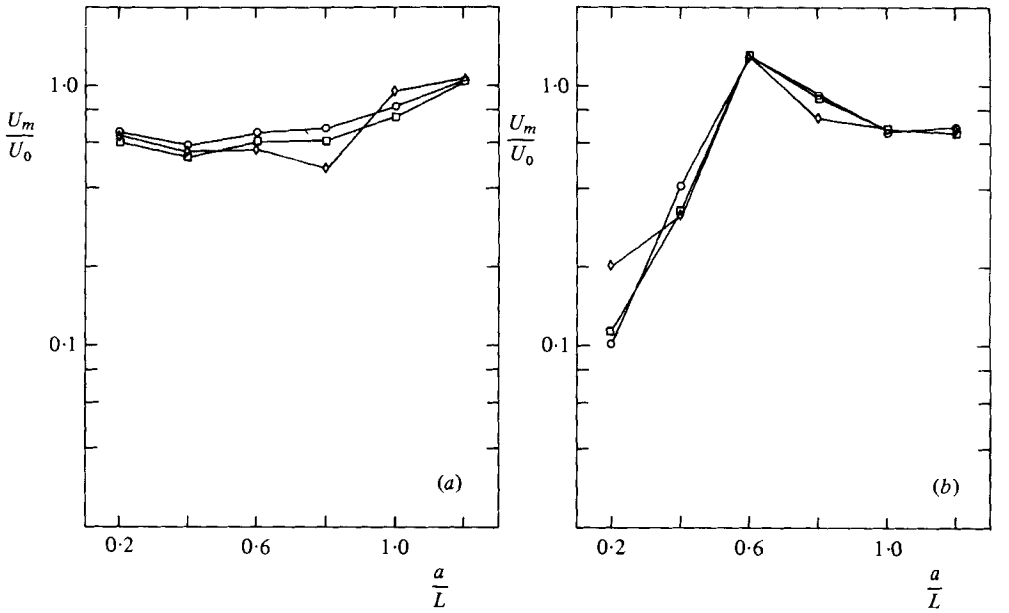

FIGURE 11. Variation with a/L of the maximum velocity at $\beta y_1 = 3$ during the course of one cycle, for various values of β/k. (*a*) Traverse A; (*b*) traverse B. Values of β/k are: □, 12; ○, 15; ◇, 20.

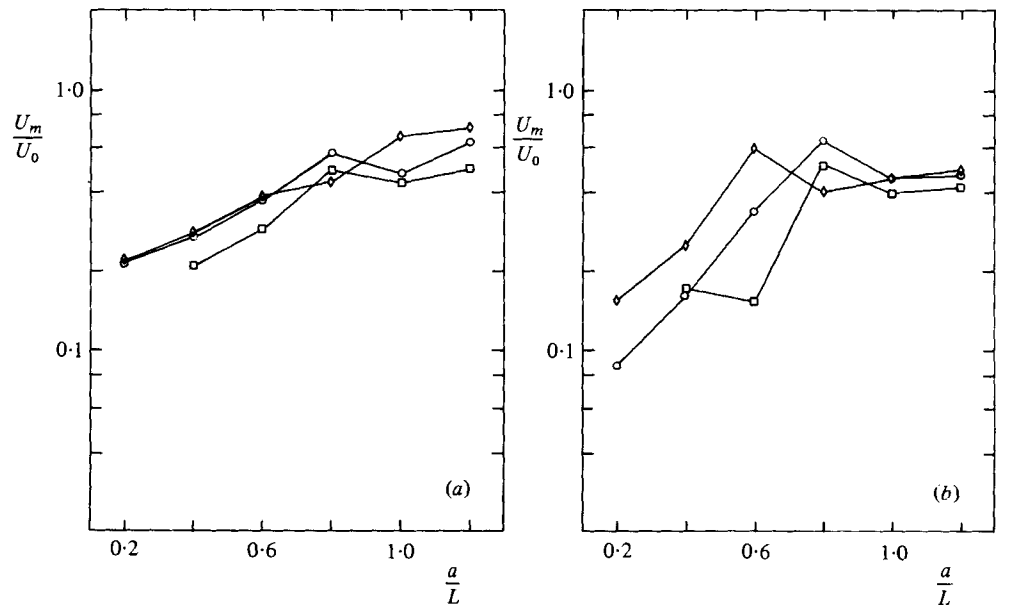

FIGURE 12. Variation with a/L of the maximum velocity at $\beta y_1 = 15$ during the course of one cycle, for various values of β/k. (*a*) Traverse A; (*b*) traverse B. For the symbols see figure 11.

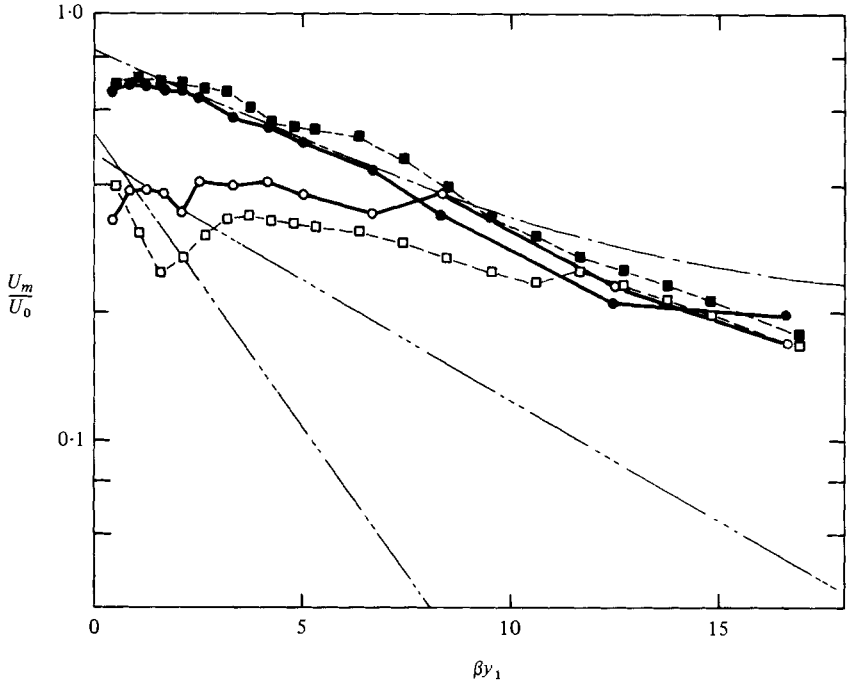

FIGURE 13. Example of the variation with βy_1 of the maximum velocity during a cycle. Self-formed ripples. $a/L = 0{\cdot}79$, $\beta/k = 10$, $h/L = 0{\cdot}13$. For the symbols see figure 7.

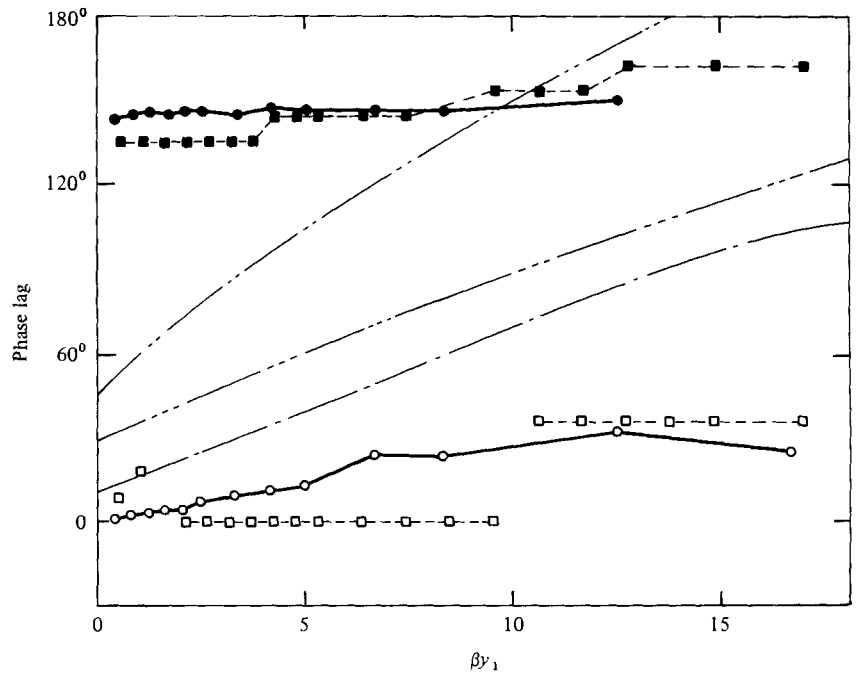

FIGURE 14. Example of the variation with βy_1 of the phase at which the maximum velocity during one cycle occurs. Self-formed ripples. $a/L = 0{\cdot}79$, $\beta/k = 10$, $h/L = 0{\cdot}13$. For the symbols see figure 13.

3.2. *Self-formed ripples in the oscillating tray rig*

The results obtained with the self-formed ripples in the oscillating tray rig are very similar, for given a/L, to those obtained with the artificial ripples. Figures 13 and 14 show an example. The value of a/L for this test was 0·79 and $h/L = 0{\cdot}13$. The flow conditions were consequently intermediate in severity between those of figure 5 and those of figure 6 and thus the reasonable agreement between Sleath's method and the experimental results is not unexpected. Kajiura's method also gives quite a good prediction of the magnitude of the maximum velocity. However, figure 14 shows that, as for the artificial ripple tests, Kajiura's prediction of phase is a long way from the experimental measurements.

For the test results shown in figures 13 and 14 the bed was active. However, the sediment movement was not intense since, otherwise, there would have been significant loss of sand from the tray.

3.3. *Self-formed ripples in the oscillating flow water channel*

It has already been pointed out that Kajiura's method gives a reasonable prediction of the amplitude of the maximum velocity with the oscillating beds but a poor prediction of the phase. The opposite appears to be the case when we are dealing with a stationary bed and an oscillating fluid as shown, for example, in figure 15. The reason is, of course, that the change from axes fixed relative to the free stream to axes fixed relative to the bed introduces a velocity component $U_\infty \cos \omega t$, where U_∞ is the amplitude of the free-stream velocity. When this component is combined with the oscillating bed velocity to obtain the fixed bed velocity the large error in phase with Kajiura's method results in a correspondingly large error in magnitude. On the other hand the error in phase of the resultant velocity is reduced.

The formulae of Kalkanis and Bakker show somewhat better agreement with the measured velocities over the trough than with those over the ripple crest, but even over the trough the agreement is not perfect. The best agreement is obtained with the method of Sleath. For those who are cynically inclined it should be pointed out that Sleath's method does not involve any empirical coefficient which can be adjusted to improve agreement with experiment. The only parameters which can be varied are a/L, β/k and h/L, and in all cases the actual experimental values for the test in question were adopted. However, figure 15 does show a small peak in the velocity record at a phase of about 130° over the crest and 170° over the trough which is not reproduced in Sleath's computed velocities. This peak corresponds to the surge in velocity as the vortex in the lee of the crest is carried back over the crest when the flow reverses. It was pointed out above that the bed profile for which computations were made should be regarded as the mean profile. During the course of a cycle the crest sways from side to side forming a small cusp of sand first on one side and then, as the flow reverses, on the other. It might be thought that the discrepancy between the experimental and computed results is due to the absence of these cusps in the bed profile assumed for the computations. However, analysis of the results for the artificial rippled bed showed the same peaks in the recorded velocity at the same points in the cycle. Since the profile of the artificial rippled bed was the same as that for which computations were made it would seem that it is not the absence of cusps in the bed profile which is responsible for the observed discrepancy.

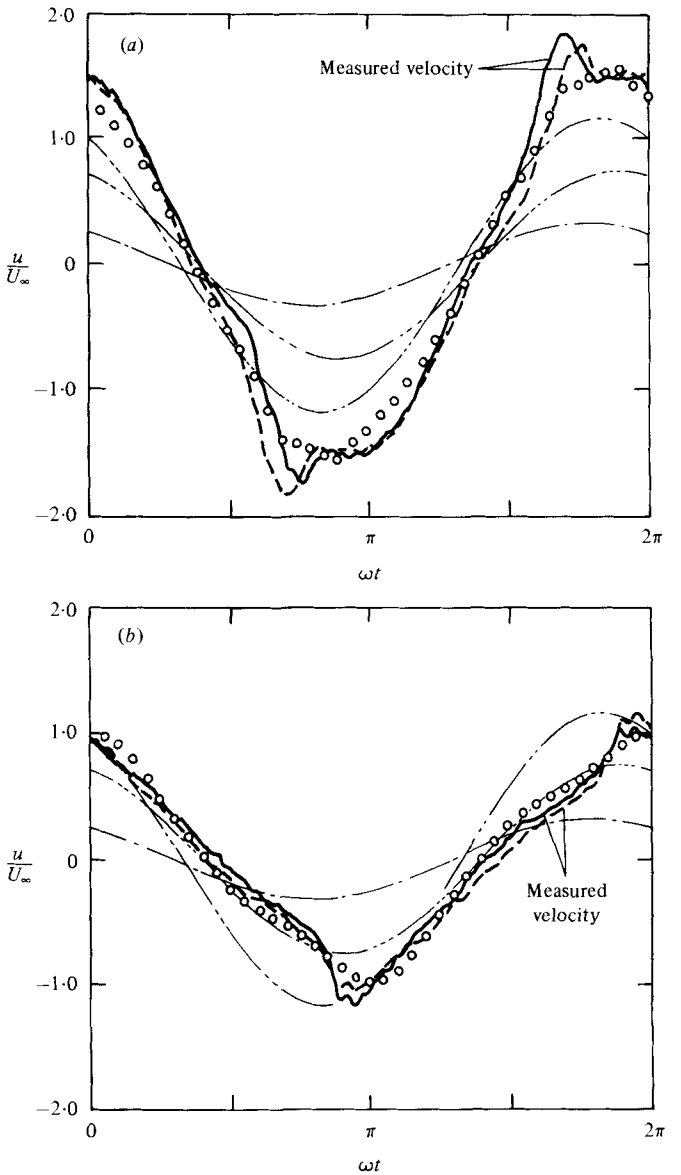

FIGURE 15. Examples of the average velocity cycle obtained with self-formed ripples in the water channel. $a/L = 0{\cdot}71$, $\beta/k = 20$, $h/L = 0{\cdot}17$. (*a*) Measured above the crest, $\beta y_1 = 1{\cdot}44$. (*b*) Measured above the trough, $\beta y_1 = 1{\cdot}18$. For the symbols see figure 5.

The way in which the amplitude and phase of the maximum velocity during the cycle vary with βy_1 is shown in figure 16 for a crest traverse and in figure 17 for a trough traverse. On the whole the best agreement between theory and experiment is obtained with Sleath's method and the least good agreement with Kajiura's. When interpreting these figures it should be remembered that at small values of βy_1 the maximum velocity is that at the small local peak shown in figure 15. Further out this local peak becomes progressively less marked.

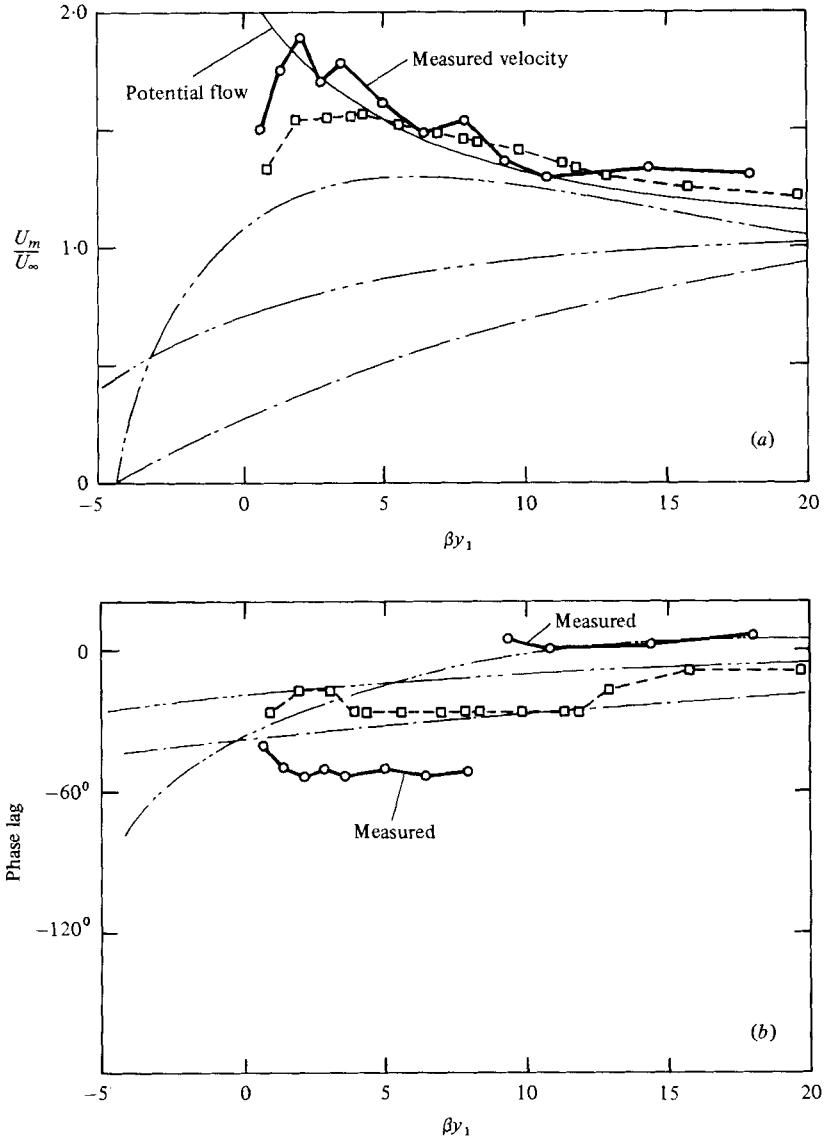

FIGURE 16. Variation with βy_1 of (*a*) the amplitude and (*b*) the phase of the maximum velocity above the ripple crest. $a/L = 0{\cdot}71, \beta/k = 20, h/L = 0{\cdot}17$. ——— – ———, Kajiura; ——— – – ———, Kalkanis; ——— – – – ———, Bakker; – – □ – –, Sleath.

The velocity potential for a stream oscillating with simple harmonic motion over a bed whose profile is given by (2) is

$$\phi = U_\infty \xi \cos \omega t, \tag{5}$$

where the velocity at infinity is $U_\infty \cos \omega t$. The variation in U_m/U_∞ for this potential flow is also shown in figures 16 and 17. Over the crest the agreement with experiment is close except, as would be expected, in the immediate vicinity of the bed. The agreement is less good over the trough since the measured velocity is strongly influenced by separation in the lee of the ripple crest which, of course, does not occur

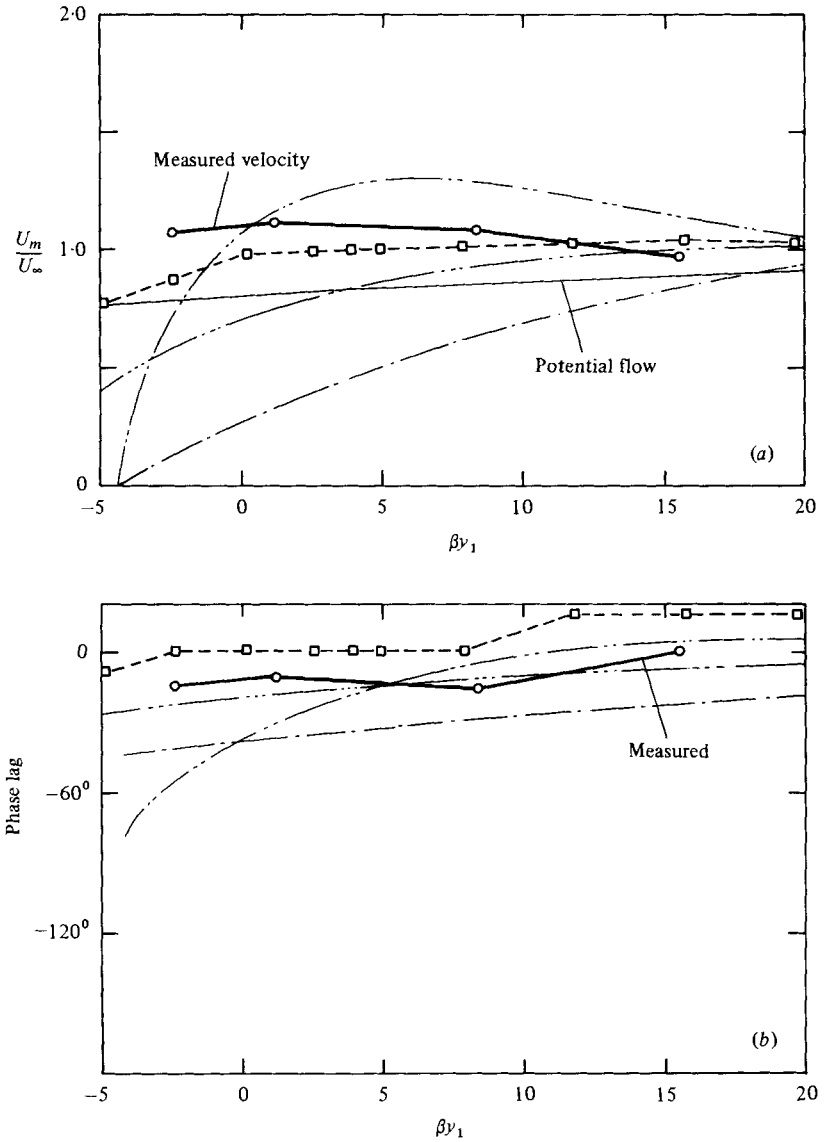

FIGURE 17. Variation with βy_1 of (*a*) the amplitude and (*b*) the phase of the maximum velocity above a ripple trough. $a/L = 0{\cdot}71$, $\beta/k = 20$, $h/L = 0{\cdot}17$. For the symbols see figure 16.

in potential flow. The variation in phase with height of the potential flow is not shown in figures 16 and 17 in order not to further confuse these figures. However, it will be seen from (5) that the phase lag of the potential flow is zero both above crest and trough. This is in reasonable agreement with the experimental results except close to the bed above the ripple crest. As pointed out above, the maximum velocity in this region is found at the small peak in the velocity record produced by the vortex carried back over the crest when the flow reverses. Since the potential flow does not show vortex formation, close agreement is hardly to be expected in this region. It may be mentioned in passing that we would expect similar agreement between the potential flow solution and the experimental results for the oscillating beds discussed

above. However, comparison in that case is complicated by the fact that the measuring point moves relative to the bed. Thus both traverses A and B correspond to measurements above both crest and trough. Also, at a fixed height the measuring point may at one instant be well away from the bed where potential flow is a reasonable approximation and subsequently very close to the bed where the approximation is poor. The comparison with the potential flow solution is thus not particularly helpful for the oscillating bed case.

So far we have discussed only the mean velocities obtained by conditional sampling of 30 recorded cycles. Figure 18 shows an example of the way in which the r.m.s. fluctuation in velocity about this mean varies during the course of a cycle. The mean velocity is also shown for comparison. The most significant feature of the r.m.s. fluctuation in velocity is the peak observed above both crest and trough at about the same point as the local peak in the mean velocity. As mentioned above, this peak is associated with the vortex carried back over the crest and then out over the trough when the flow reverses. However, apart from these peaks the r.m.s. fluctuation in velocity remains fairly constant during the course of the cycle. Figure 19 shows the way in which the mean value of the r.m.s. fluctuations, averaged over a complete cycle, varies with height above the bed. The general form of the variation with height is similar to that observed by Sleath (1975*a*) at much lower values of Reynolds number. Sleath suggested that the length scale of fluctuations in velocity was comparable with ripple length and height, rather than with the much smaller scales normally associated with turbulence. This conclusion appears to be supported by the way in which the r.m.s. fluctuation at a given height is almost identical above both crest and trough.

A much more severe test of the agreement between theory and experiment is provided by measurements of the Eulerian drift velocities in the vicinity of the ripple crest. In an oscillatory flow water channel there is, in theory, no net drift of the sort associated with progressive waves. However, each ripple sets up its own re-circulating drift pattern. Figure 20 shows measurements of the horizontal component of the Eulerian drift velocity for four vertical traverses. One traverse was over the ripple crest, one over a trough and the other two traverses were equally spaced between crest and trough. By symmetry, there should be no net flow over either crest or trough and consequently the measurements shown in figure 20(*a*) provide an indication of the degree of experimental error. Of the four methods for calculating velocity discussed above, only that due to Sleath predicts a re-circulating drift in the vicinity of the ripple. Figure 20(*b*) shows that the measured drifts are significantly stronger than those calculated from Sleath's method but the general variation with height is the same. In particular, we see a strong drift towards the adjacent ripple crest in the immediate vicinity of the bed and a corresponding drift away from the ripple crest further out. Since a net drift of fluid near the bed will also produce a net drift of sediment, these measurements throw some light on vortex ripple formation in oscillatory flow.

The test results shown in figures 15–20 are all for $\beta/k = 20$. Tests were also carried out at other values of β/k but, as for the artificial ripple tests, the variation with β/k was found to be relatively small. It was, unfortunately, not possible to investigate the effect of varying a/L because all of the stable ripples obtained in this rig had very similar values of this parameter.

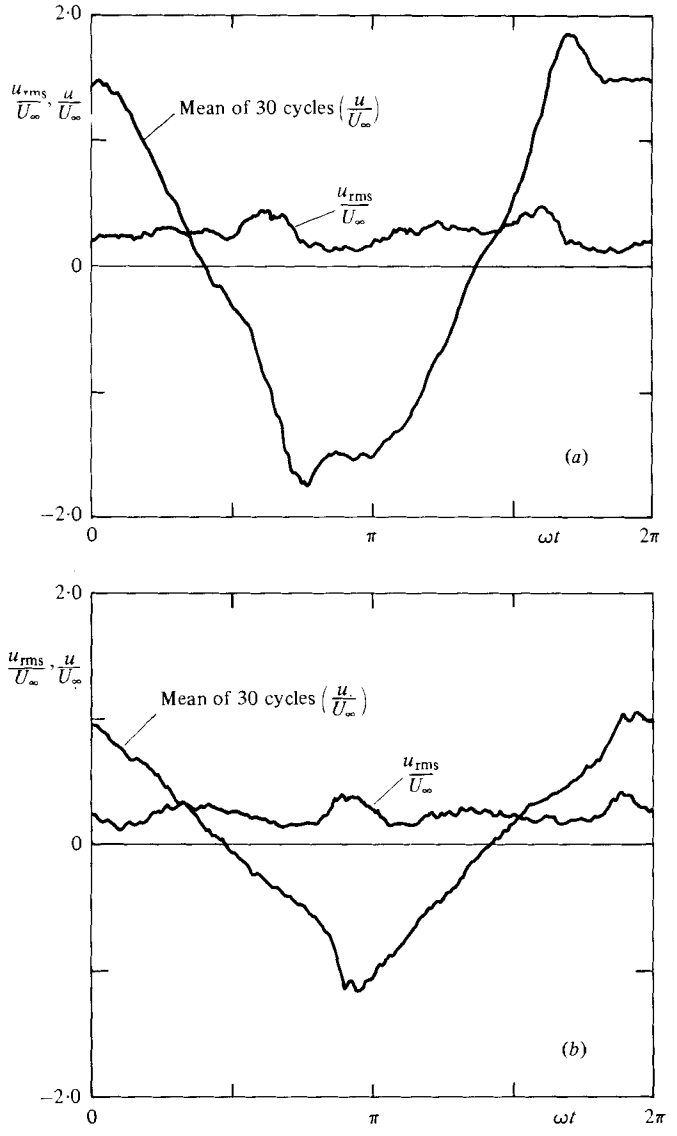

FIGURE 18. Examples of the variation of the r.m.s. fluctuation in velocity, u_{rms}, during the course of one cycle. $a/L = 0{\cdot}71, \beta/k = 20, h/L = 0{\cdot}17$. (*a*) Measured above the crest, $\beta y_1 = 1{\cdot}44$. (*b*) Measured above the trough, $\beta y_1 = 1{\cdot}18$.

The measurements with self-formed ripples which have been discussed so far have been for low or moderate sediment transport rates, as will have been gathered from the quoted values of a/L and h/L (at high sediment transport rates a/L increases and h/L decreases). Figure 21 shows an example of the sort of result obtained when there is intense sediment motion. This test was carried out with Perspex beads of median diameter 0·6 mm whereas all of the self-formed ripple tests discussed above were with 0·41 mm sand. At these very high sediment transport rates it was found necessary to roughen the floor of the water channel with a layer of gravel in order to prevent slipping of the bed of sediment. However, the depth of sediment was sufficiently great for the gravel to be covered by at least 10 mm of stationary Perspex beads (underneath the

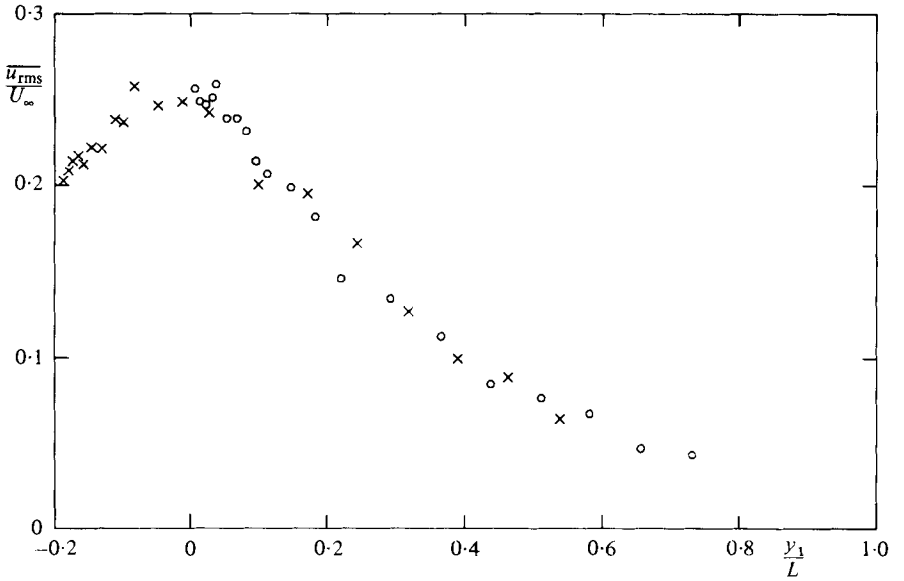

FIGURE 19. Variation with distance from the bed of the mean value during one cycle of the r.m.s. fluctuation in velocity. $a/L = 0{\cdot}74$, $\beta/k = 20$, $h/L = 0{\cdot}20$. ○, measured above the crest; ×, measured above the trough.

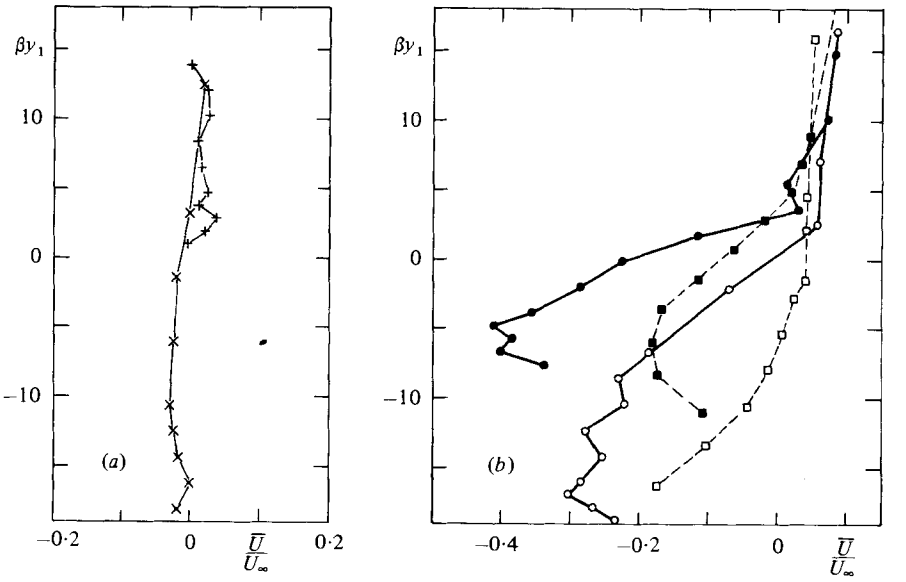

FIGURE 20. Variation with height of the horizontal component of the Eulerian drift velocity. $a/L = 0{\cdot}74$, $\beta/k = 20$, $h/L = 0{\cdot}20$. ×, measured above the trough; +, measured above the crest; ●, measured at $\frac{1}{6}L$ from the crest; ■, Sleath, $\frac{1}{6}L$ from the crest; ○, measured at $\frac{1}{3}L$ from the crest; □, Sleath, $\frac{1}{3}L$ from the crest.

moving layers) at all times. Under these test conditions the bed appeared plane except close to the moment of flow reversal. At this point in the cycle vortex formation appeared to occur throwing up clouds of sediment from the bed. However, for the most part, the moving sediment was confined to a layer about 20 mm thick with clear

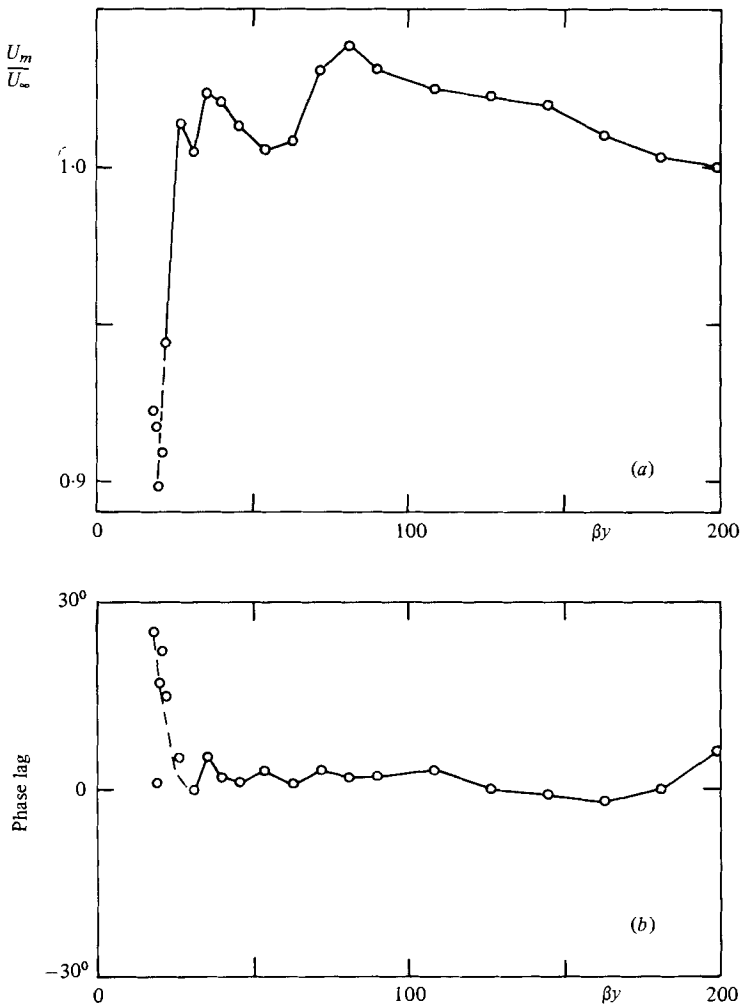

FIGURE 21. Variation with distance above the bed of (*a*) the magnitude and (*b*) the phase of the maximum velocity. Quasi-flat bed. $U_0/(\omega\nu)^{\frac{1}{2}} = 381{\cdot}7$.

water immediately above. With the existing equipment velocity measurements could not be extended down into the layer of moving sediment. Nevertheless, a certain number of conclusions may be drawn from the measurements shown in figure 21. Although the bed appeared plane during most of the cycle and although the flow above the layer of sediment appeared laminar, the velocity distribution in figure 21 (*a*) is significantly different from that for a smooth bed in laminar flow even if the no-slip condition at the bed is relaxed. For the fixed smooth bed the maximum velocity occurs at $\beta y = 2{\cdot}3$ and is 7 % greater than the free stream velocity. Even when allowance is made for the uncertainty as to what should be taken as the bed level, the maximum velocity in figure 21 (*a*) occurs at a value of βy of at least 60 and the overshoot is only about 4 %. The variation in phase shown in figure 21 (*b*) is also very different from that for a smooth bed. In particular, the measurements very close to the bed show a phase lag of about 20° whereas for a smooth bed in laminar flow the phase lag is nowhere greater than 1°. There are various possible explanations for

these differences. Firstly, although the bed appeared plane there may in reality have been very low-amplitude ripples obscured by the layer of moving sediment. Secondly, the vortex formation at the end of each half cycle would be expected to have some effect. Thirdly, the well-known dilatation of a layer of sediment when motion takes place may also have had an effect since most of the sediment came to rest at the end of each half cycle. This resulted in the top of the sediment layer 'breathing' up and down during the course of each half cycle. Finally, turbulence may also have been important even though the flow appeared laminar.

The authors would like to thank the NERC for a generous grant for the purchase of equipment. One of the authors (C.G.D.T.) would like to acknowledge the financial support of the Sir Henry Strakosch Trust and the South African CSIR.

Appendix

The experimental data is compared with the predictions obtained from the methods of Kalkanis (1964), Kajiura (1968), Bakker (1974) and Sleath (1974). Since the publications in which these methods are set out are not always widely available a brief summary of the basic assumptions is given below.

(*a*) *Kalkanis* (1964)

This is a purely empirical formula based on velocity measurements close to rough beds oscillating in their own plane in a tank of water. The bed in the case of the two-dimensional roughness consisted of round or half-round rods.

(*b*) *Kajiura* (1968)

If the mean flow is assumed to be parallel to the bed the equation of motion may be reduced to

$$\frac{\partial u}{\partial t} = -\frac{1}{\rho}\frac{\partial p}{\partial x} + \frac{\partial \tau}{\partial y}, \tag{A 1}$$

where p is pressure. Kajiura assumes that the shear stress τ may be expressed as

$$\tau = \rho\epsilon\frac{\partial u}{\partial y}, \tag{A 2}$$

where ϵ is an eddy viscosity which, for rough beds, varies as follows

$$\begin{aligned} \epsilon &= 1{\cdot}354\,Ku_* k_s \quad \text{for} \quad 0 \leqslant y < \tfrac{1}{2}k_s, \\ \epsilon &= Ku_* y \quad \text{for} \quad \tfrac{1}{2}k_s \leqslant y < d, \\ \epsilon &= Ku_* d \quad \text{for} \quad d \leqslant y, \end{aligned} \tag{A 3}$$

where u_* is the maximum value of $(\tau/\rho)^{\frac{1}{2}}$ at the bed, K is the Kármán constant and d is the upper limit of the overlap layer. Kajiura also assumes that the shear stress varies sinusoidally with time. Consequently, substitution of (A 2) and (A 3) into (A 1) produces a relationship which may be solved analytically.

(*c*) *Bakker* (1974)

Bakker, too, makes use of equation (A 1). However, he considers only turbulent flow and assumes that the shear stress τ may be approximated by the Reynolds stress. Following Prandtl and von Kármán he takes

$$\tau = \rho l^2 \frac{\partial u}{\partial y}\left|\frac{\partial u}{\partial y}\right| \tag{A 4}$$

where the mixing length l is given by

$$l = Ky. \tag{A 5}$$

Substituting from (A 4) and (A 5) into (A 1) and assuming that $\partial p/\partial x$ is constant across the boundary layer gives an expression which may be solved numerically. The shear velocity is assumed to vary sinusoidally with time at $y = 0$.

(*d*) *Sleath* (1974)

This method consists essentially of a numerical solution of the two-dimensional vorticity equation obtained by cross-differentiation of the Navier Stokes equations to eliminate pressure. The viscosity is assumed to have the value appropriate for laminar flow, i.e. no use is made of eddy viscosity or mixing length.

REFERENCES

Bagnold, R. A. 1946 Motion of waves in shallow water. Interaction of waves and sand bottoms. *Proc. Roy. Soc.* A **187**, 1–15.

Bakker, W. T. 1973 Bottom friction and velocity distribution in an oscillatory flow. *Rijkswaterstaat, Dir. Hydr. Res. & Water Management, Dept. Coastal Res., Memo* 72–23.

Bakker, W. T. 1974 Sand concentration in an oscillatory flow. *Proc. 14th Conf. Coastal Engng, Copenhagen*, pp. 1129–1148.

Bakker, W. T. & Van Doorn, Th. 1978 Near-bottom velocities in waves with a current. *Proc. 16th Conf. Coastal Engng, Hamburg*, pp. 1394–1413.

Beech, N. W. 1978 Boundary layers due to gravity waves. Ph.D. thesis, University of Nottingham.

Du Toit, C. G. 1980 Velocities close to a bed of sand in oscillatory flow. Ph.D. thesis, University of Cambridge.

Greated, C. C. & Manning, R. 1970 Water waves measured with a laser flowmeter. *La Houille Blanche* **25**, 567–570.

Horikawa, K. & Watanabe, W. 1968 Laboratory study on oscillatory boundary layer flow. *Coastal Engng, Japan* **11**, 13–28.

Jonsson, I. G. 1963 Measurements in the turbulent wave boundary layer. *Proc. 10th IAHR Congress, London*, 112, pp. 85–92.

Jonsson, I. G. 1980 A new approach to oscillatory rough turbulent boundary layers. *Ocean Engng* **7**, 109–152.

Jonsson, I. G. & Carlsen, N. A. 1976 Experimental and theoretical investigations in an oscillatory turbulent boundary layer. *J. Hydraulic Res.* **14**, 45–60.

Kajiura, K. 1968 A model of the bottom boundary in water waves. *Bull. Earthquake Res. Inst.* **46**, 75–123.

Kalkanis, G. 1957 Turbulent flow near an oscillating wall. *U.S. Army B.E.B., Tech. Memo* no. 97.

Kalkanis, G. 1964 Transport of bed material due to wave action. *U.S. Army Coastal Engng Res. Center, Tech. Memo* no. 2.

Kamphuis, J. W. 1975 Friction factor under oscillatory waves. *Proc. A.S.C.E. J. Waterways, Harbors & Coastal Engng Div.* **101** (WWZ), 135–144.

KANEKO, A. & HONJI, H. 1979 Double structures of steady streaming in the oscillatory viscous flow over a wavy wall. *J. Fluid Mech.* **93**, 727–736.

LONGUET-HIGGINS, M. S. 1981 Oscillating flow over steep sand ripples. *J. Fluid Mech.* **107**, 1–35.

LYNE, W. H. 1971 Unsteady viscous flow over a wavy wall. *J. Fluid Mech.* **50**, 33–48.

MACDONALD, T. C. 1973 Sediment transport due to oscillatory waves. *Univ. California, Hyd. Eng. Lab. Tech. Rep.* HEL-2-39.

MANNING, R. 1971 On laser doppler measurements to record bed velocities at a harbour bar model. *Proc. 14th IAHR Cong., Paris*, vol. 4, pp. 1–10.

MOTZFELDT, H. 1937 Die turbulente Strömung an welligen Wanden. *Z. angew. Math. Mech.* **17**, 193–212.

NAKATO, T., LOCHER, F. A., GLOVER, J. R. & KENNEDY, J. F. 1977 Wave entrainment of sediment from rippled beds. *Proc. A.S.C.E., J. Waterways, Port, Coastal & Ocean Engng Div.* **103** (WW1), 83–99.

SLEATH, J. F. A. 1970 Velocity measurements close to the bed in a wave tank. *J. Fluid Mech.* **42**, 111–123.

SLEATH, J. F. A. 1974 Velocities above a rough bed in oscillatory flow. *Proc. A.S.C.E., J. Waterways, Harbors & Coastal Engng Div.* **100** (WW4), 287–304.

SLEATH, J. F. A. 1975*a* A contribution to the study of vortex ripples. *J. Hydraulic Res.* **13**, 315–328.

SLEATH, J. F. A. 1975*b* Transition in oscillatory flow over rippled beds. *Proc. Inst. Civil Eng.* **59**, 309–332.

STOKES, G. G. 1851 On the effect of internal friction of fluids on the motion of pendulums. *Trans. Camb. Phil. Soc.* **9**, 20–21.